
FUZZY C-MEANS CLUSTERING FOR PERSISTENCE DIAGRAMS

Thomas Davies

University of Southampton

t.o.m.davies@soton.ac.uk

Jack Aspinall

University of Oxford

jack.aspinall@materials.ox.ac.uk

Bryan Wilder

Harvard University

bwilder@g.harvard.edu

Long Tran-Thanh

University of Warwick

long.tran-thanh@warwick.ac.uk

ABSTRACT

Persistence diagrams concisely represent the topology of a point cloud whilst having strong theoretical guarantees. Most current approaches to integrating topological information into machine learning implicitly map persistence diagrams to a Hilbert space, resulting in deformation of the underlying metric structure whilst also generally requiring prior knowledge about the true topology of the space. In this paper we give an algorithm for Fuzzy c-Means (FCM) clustering directly on the space of persistence diagrams, enabling unsupervised learning that automatically captures the topological structure of data, with no prior knowledge or additional processing of persistence diagrams. We prove the same convergence guarantees as traditional FCM clustering: every convergent subsequence of iterates tends to a local minimum or saddle point. We end by presenting experiments where our fuzzy topological clustering algorithm allows for unsupervised top- k candidate selection in settings where (i) the properties of persistence diagrams make them the natural choice over geometric equivalents, and (ii) the probabilistic membership values let us rank candidates in settings where verifying candidate suitability is expensive: lattice structure classification in materials science and pre-trained model selection in machine learning.

1 INTRODUCTION

Persistence diagrams, a concise representation of the topology of a point cloud with strong theoretical guarantees, have emerged as a new tool in the field of data analysis (Edelsbrunner & Harer, 2010). Persistence diagrams have been successfully used to analyse problems ranging from financial crashes (Gidea & Katz, 2018) to protein binding (Kovacev-Nikolic et al., 2014), but the non-Hilbertian nature of the space of persistence diagrams means it is difficult to directly use persistence diagrams for machine learning. In order to better integrate diagrams into machine learning workflows, efforts have been made to map them into a more manageable form; primarily through embeddings into finite feature vectors, functional summaries, or by defining a positive-definite kernel on diagram space. In all cases, this explicitly or implicitly embeds diagrams into a Hilbert space which deforms the metric structure, potentially losing important information. With the exception of Topological Autoencoders, techniques to integrate these persistence-based summaries as topological regularisers and loss functions currently require prior knowledge about the correct topology of the dataset, which is clearly not feasible in most scenarios.

Against this background, we give an algorithm to perform Fuzzy c-Means (FCM) clustering (Bezdek, 1980) *directly* on collections of persistence diagrams, giving an important unsupervised learning algorithm and enabling learning from persistence diagrams without deforming the metric structure. We perform the convergence analysis for our algorithm, giving the same guarantees as traditional FCM clustering: that every convergent subsequence of iterates tends to a local minimum or saddle point. We demonstrate the value of our fuzzy clustering algorithm by using it to cluster datasets that benefit from both the topological and fuzzy nature of our algorithm. We apply our technique

in two settings: lattice structures in materials science and the decision boundaries of CNNs. A key property for machine learning in materials science has been identified as “invariance to the basis symmetries of physics [...] rotation, reflection, translation” (Schmidt et al., 2019). Geometric clustering algorithms do not have this invariance, but persistence diagrams do, making them ideally suited for this application; we can cluster transformed lattice structure datasets where geometric equivalents fail. In addition to this, our probabilistic membership values allow us to rank the top- k most likely lattices assigned to a cluster. This is particularly important in materials science, as further investigation requires expensive laboratory time and expertise. Our second application is inspired by Ramamurthy et al. (2019), who show that models perform better on tasks if they have topologically similar decision boundaries. We use our algorithm to cluster models and tasks by the persistence diagrams of their decision boundaries. Not only is our algorithm able to successfully cluster models to the correct task, based just on the topology of its decision boundary, but we show that higher membership values imply better performance on unseen tasks.

1.1 RELATED WORK

Means of persistence diagrams. Our work relies on the existence of statistics in the space of persistence diagrams. Mileyko et al. (2011) first showed that means and expectations are well-defined in the space of persistence diagrams. Specifically, they showed that the Fréchet mean, an extension of means onto metric spaces, is well-defined under weak assumptions on the space of persistence diagrams. Turner et al. (2012) then developed an algorithm to compute the Fréchet mean. We adapt the algorithm by Turner et al. to the weighted case, but the combinatoric nature of their algorithm makes it computationally intense. Lacombe et al. (2018) framed the computation of means and barycentres in the space of persistence diagram as an optimal transport problem, allowing them to use the Sinkhorn algorithm (Cuturi & Doucet, 2014) for fast computation of approximate solutions. The vectorisation of the diagram required by the algorithm by Lacombe et al. makes it unsuitable for integration into our work, as we remain in the space of persistence diagrams. Techniques to speed up the matching problem fundamental to our computation have also been proposed by Vidal et al. (2020) and Kerber et al. (2017).

Learning with persistence-based summaries. Integrating diagrams into machine learning workflows remained challenging even with well-defined means, as the space is non-Hilbertian (Turner & Spreemann, 2019). As such, efforts have been made to map diagrams into a Hilbert space; primarily either by embedding into finite feature vectors (Kališnik, 2018; Fabio & Ferri, 2015; Chepushtanova et al., 2015) or functional summaries (Bubenik, 2015; Rieck et al., 2019), or by defining a positive-definite kernel on diagram space (Reininghaus et al., 2015; Carrière et al., 2017; Le & Yamada, 2018). These vectorisations have been integrated into deep learning either by learning parameters for the embedding (Hofer et al., 2017; Carrière et al., 2020; Kim et al., 2020; Zhao & Wang, 2019; Zieliński et al., 2019), or as part of a topological loss or regulariser (Chen et al., 2018; Gabrielsson et al., 2020; Clough et al., 2020; Moor et al., 2019). However, the embeddings used in these techniques deform the metric structure of persistence diagram space (Bubenik & Wagner, 2019; Wagner, 2019; Carrière & Bauer, 2019), potentially leading to the loss of important information. Furthermore, these techniques generally require prior knowledge of a ‘correct’ target topology which cannot plausibly be known in most scenarios. In comparison, our algorithm acts in the space of persistence diagrams so it does not deform the structure of diagram space via embeddings, and is entirely unsupervised, requiring no prior knowledge about the topology.

Hard clustering. Maroulas et al. (2017) gave an algorithm for hard clustering persistence diagrams based on the algorithm by Turner et al. Lacombe et al. (2018) gave an alternate implementation of hard clustering based on their algorithm for barycentre computation, providing a computational speed-up over previous the work by Maroulas et al. The primary advantages of our work over previous work on hard clustering are as follows.

- (i) The probabilistic membership values allow us to rank datasets in the cluster, enabling top- k candidate selection in settings where verifying correctness is expensive. The value provided by this fuzzy information is demonstrated in the experiments.
- (ii) The fuzzy membership values provide information about proximity to all clusters, whereas hard labelling loses most of that information. In our experiments we demonstrate that this additional information can be utilised in practice.

- (iii) The weighted cost function makes the convergence analysis (which we provide) entirely non-trivial in comparison to the non-fuzzy case. We consider this convergence analysis a primary contribution of our paper.
- (iv) Fuzzy membership values have been shown to be more robust to noise than discrete labels (Klawonn, 2004).
- (v) Unlike hard clustering, fuzzy clustering is analytically differentiable, allowing integration of the fuzzy clustering step into deep learning methods (Wilder et al., 2019).

Geometric equivalents. The most similar unsupervised learning technique to our algorithm is Wasserstein Barycentre Clustering (WBC). It clusters datasets of point clouds by the Wasserstein distance between the point clouds, rather than the Wasserstein distance between their persistence diagrams. We compare our algorithm experimentally to WBC using ADMM (Ye & Li, 2014), Bregman ADMM (Ye et al., 2017), Subgradient Descent (Cuturi & Doucet, 2014), Iterative Bregman Projection (Benamou et al., 2015), and full linear programming (Li & Wang, 2008). Each of these algorithms computes or approximates the Wasserstein barycentre in different ways. Theoretically, fuzzy discrete distribution clustering (d. A. T. de Carvalho et al., 2015) is similar to our algorithm, but the addition of the diagonal in the persistence diagram makes our work distinct.

1.2 OUR CONTRIBUTIONS

1. Our main contribution is an algorithm for Fuzzy c-Means clustering of persistence diagrams, along with the convergence analysis. Given a collection of persistence diagrams $\mathbb{D}_1, \dots, \mathbb{D}_n$, we alternatively calculate cluster centres $\mathbb{M}_1, \dots, \mathbb{M}_c$ and membership values $r_{jk} \in [0, 1]$ which denote the degree to which diagram \mathbb{D}_j is associated with cluster \mathbb{M}_k . We prove Theorem 1, showing that every convergent subsequence of these alternative update steps tends to a local minimum or saddle point of the cost function. This is the same convergence guarantee provided by traditional FCM clustering (Bezdek et al., 1987), but requires additional work as the space of persistence diagrams with the Wasserstein distance has far weaker theoretical properties than Euclidean space.
2. Updating the cluster centres requires computing the weighted Fréchet mean. We extend the algorithm given by Turner et al. (2012) to the weighted case, justifying our addition of weights by extending their proof to show that the updated algorithm converges.
3. We implement our algorithm in Python, available at <https://github.com/tomogwen/fpdcluster>. It works with persistence diagrams from commonly used open-source libraries for Topological Data Analysis (TDA),¹ so is available for easy integration into current workflows, offering a powerful unsupervised learning algorithm to data science practitioners using TDA.
4. We demonstrate the application of our algorithm to settings where (i) the properties of persistence diagrams makes clustering them the natural choice over geometric equivalents and (ii) the probabilistic membership values can be used to rank candidates for top- k selection. Our algorithm classifies transformed lattice structures from materials science where geometric equivalents fail, whilst giving probabilistic rankings to help prioritise expensive further investigation. We also cluster the persistence diagrams of decision boundaries and labelled datasets, showing that our fuzzy clustering captures information about model performance on unseen tasks.

2 TOPOLOGICAL PRELIMINARIES

Topological Data Analysis emerged from the study of algebraic topology, providing a toolkit to fully describe the topology of a dataset. We offer a quick summary below; for more comprehensive details see Edelsbrunner & Harer (2010). A set of points in \mathbb{R}^d are indicative of the shape of the distribution they are sampled from. By connecting points that are pairwise within $\epsilon > 0$ distance of each other, we can create an approximation of the distribution called the Vietoris-Rips complex (Vietoris, 1927). Specifically, we add the convex hull of any collection of points that are pairwise at most ϵ apart to the ϵ -Vietoris-Rips complex. However, choosing an ϵ remains problematic; too low a value and key points can remain disconnected, too high a value and the points become fully connected. To overcome this we use *persistence*: we consider the approximation over all values of ϵ simultaneously,

¹Dionysus and Ripser (Bauer, 2019).

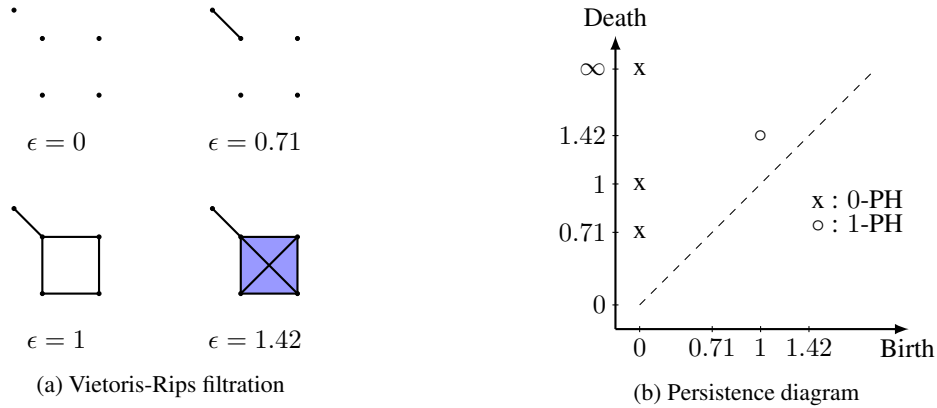


Figure 1: An example Vietoris-Rips filtration with its persistence diagram. We only add convex hulls when points are pairwise ϵ apart, so there is a hole at $\epsilon = 1$ whilst the diagonals of the square are not close enough to fill the hole in. This hole can be seen as a point at $(1, 1.42)$ in the 1-PH persistence diagram.

and study how the topology of that approximation evolves as ϵ grows large. We call the collection of complexes for all ϵ a filtration.

For each ϵ , we compute the p -homology group. This tells us the topology of the ϵ -Vietoris-Rips complex: the 0-homology counts the number of connected components, the 1-homology counts the number of holes, the 2-homology counts the number of voids, etc. (Edelsbrunner et al., 2000). The p -persistent homology (p -PH) group is created by summing the p -homology groups over all ϵ . This results in a p -PH group that summarises information about the topology of the dataset at all granularities. If a topological feature, such as a connected component or hole, persists throughout a large range of granularities, then it's more likely to be a feature of the distribution. If it only persists for a short amount of time, then it's more likely to be noise (Cohen-Steiner et al., 2007). We can stably map a p -PH group into a multiset in the extended plane called a persistence diagram (Chazal et al., 2012). Each topological feature has a birth and death: a feature is born when it enters the complex, and dies when the complex grows enough to destroy it. For example, in Figure 1(a), a feature is born at $\epsilon = 1$ when four lines form a hole. This feature dies at $\epsilon = 1.42$ when the hole is filled in. This is shown in the persistence diagram in Figure 1(b) as a point at $(1, 1.42)$ in 1-PH. By computing the birth/death points for each topological feature in the filtration, we get a complete picture of the topology of the point cloud at all granularities (Zomorodian & Carlsson, 2005). The persistence diagram is the collection of birth/death points, along with the diagonal $\Delta = \{(a, a) : a \in \mathbb{R}\}$ with infinite multiplicity, added in order to make the space of persistence diagrams complete (Mileyko et al., 2011).

3 ALGORITHMIC DESIGN

3.1 CLUSTERING PERSISTENCE DIAGRAMS

In order to cluster we need a distance on the space of persistence diagrams. We use the 2-Wasserstein L_2 metric as it is stable on persistence diagrams of finite point clouds (Chazal et al., 2012). The Wasserstein distance is an optimal transport metric that has found applications across machine learning. In the Euclidean case, it quantifies the smallest distance between optimally matched points. Given diagrams $\mathbb{D}_1, \mathbb{D}_2$, the distance is

$$W_2(\mathbb{D}_1, \mathbb{D}_2) = \left(\inf_{\gamma: \mathbb{D}_1 \rightarrow \mathbb{D}_2} \sum_{x \in \mathbb{D}_1} \|x - \gamma(x)\|_2^2 \right)^{1/2},$$

where the infimum is taken over all bijections $\gamma : \mathbb{D}_1 \rightarrow \mathbb{D}_2$. Note that as we added the diagonal with infinite multiplicity to each diagram, these bijections exist. If an off-diagonal point is matched to the diagonal the transportation cost is simply the shortest distance to the diagonal. In fact, the closer a

point is to the diagonal, the more likely it is to be noise (Cohen-Steiner et al., 2007), so this ensures our distance is not overly affected by noise.

We work in the space $\mathcal{D}_{L^2} = \{\mathbb{D} : W_2(\mathbb{D}, \Delta) < \infty\}$,² as this leads to a geodesic space with known structure (Turner et al., 2012). Given a collection of persistence diagrams $\{\mathbb{D}_j\}_{j=1}^n \subset \mathcal{D}_{L^2}$ and a fixed number of clusters c , we wish to find cluster centres $\{\mathbb{M}_k\}_{k=1}^c \subset \mathcal{D}_{L^2}$, along with membership values $r_{jk} \in [0, 1]$ that denote the extent to which \mathbb{D}_j is associated with cluster \mathbb{M}_k . We follow probabilistic fuzzy clustering, so that $\sum_k r_{jk} = 1$ for each j .

We extend the FCM algorithm originally proposed by Bezdek (1980). Our r_{jk} is the same as traditional FCM clustering, adapted with the Wasserstein distance. That is,

$$r_{jk} = \left(\sum_{l=1}^c \frac{W_2(\mathbb{M}_k, \mathbb{D}_j)}{W_2(\mathbb{M}_l, \mathbb{D}_j)} \right)^{-1}. \quad (1)$$

To update \mathbb{M}_k , we compute the weighted Fréchet mean $\hat{\mathbb{D}}$ of the persistence diagrams $\{\mathbb{D}_j\}_{j=1}^n$ with the weights $\{r_{jk}^2\}_{j=1}^n$. Specifically,

$$\mathbb{M}_k \leftarrow \arg \min_{\hat{\mathbb{D}}} \sum_{j=1}^n r_{jk}^2 W_2(\hat{\mathbb{D}}, \mathbb{D}_j)^2, \text{ for } k = 1, \dots, c. \quad (2)$$

As the weighted Fréchet mean extends weighted centroids to general metric spaces, this gives our fuzzy cluster centres. The computation of the weighted Fréchet mean is covered in Section 3.2. By alternatively updating (1) and (2) we get a sequence of iterates. Theorem 1, proven in Appendix A, provides the same convergence guarantees as traditional FCM clustering.

Theorem 1. *Every convergent subsequence of the sequence of iterates obtained by alternatively updating membership values and cluster centres with (1) and (2) tends to a local minimum or saddle point of the cost function $J(R, \mathbb{M}) = \sum_{j=1}^n \sum_{k=1}^c r_{jk}^2 W_2(\mathbb{M}_k, \mathbb{D}_j)^2$.*

Observe that we only guarantee the convergence of subsequences of iterates. This is the same as traditional FCM clustering, so we follow the same approach to a stopping condition and run our algorithm for a fixed number of iterations. The entire algorithm is displayed in Algorithm 1.

Algorithm 1 FPDCluster

Input Diagrams $\mathbb{D} = \{\mathbb{D}_j\}_{j=1}^n$, number of clusters c , maximum iterations MAXITER
Output Cluster centres $\mathbb{M} = \{\mathbb{M}_k\}_{k=1}^c$, membership values $R = \{r_{jk}\}$

1: $\mathbb{D} = \text{ADDIAGONALS}(\mathbb{D})$	7: end for
2: $\mathbb{M} = \text{INITCENTRES}(\mathbb{D})$	8: end for
3: for count in $1.. \text{MAXITER}$ do	9: for k in $1..c$ do
4: for j in $1..n$ do	10: $\mathbb{M}_k \leftarrow \text{WFRECHETMEAN}(\mathbb{D}, R_k)$
5: for k in $1..c$ do	11: end for
6: $r_{jk} \leftarrow \left(\sum_{l=1}^c \frac{W_2(\mathbb{M}_k, \mathbb{D}_j)}{W_2(\mathbb{M}_l, \mathbb{D}_j)} \right)^{-1}$	12: end for
	13: return \mathbb{M}, R

3.2 COMPUTING THE WEIGHTED FRÉCHET MEAN

Turner et al. (2012) give an algorithm for the computation of Fréchet means. In this section we extend their algorithm and proof of convergence to the weighted case. In Algorithm 1 we add copies of the diagonal to ensure that each diagram has the same cardinality; denote this cardinality

²To ensure that our persistence diagrams are all in this space, we map points at infinity to a hyperparameter T that is much larger than other death values in the diagram. This hyperparameter ensures that the one point at infinity will always be matched to the corresponding point at infinity when computing the Wasserstein distance between diagrams. This can be avoided entirely by computing the diagrams with extended persistence (Cohen-Steiner et al., 2009), which removes points at infinity.

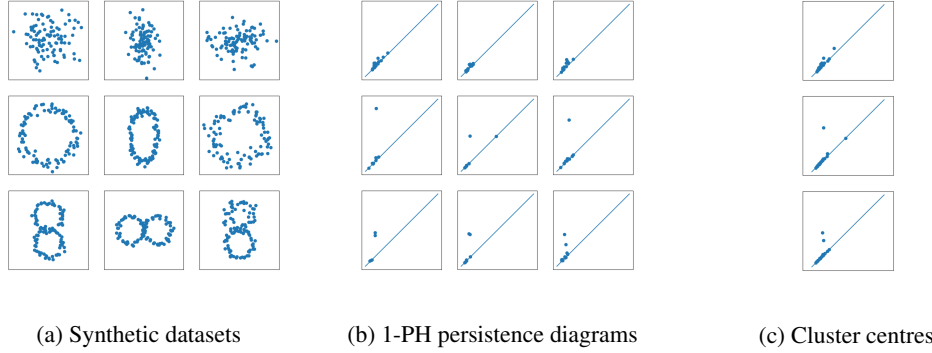


Figure 2: Our algorithm successfully clustered the persistence diagrams, finding cluster centres that represent the topology of the datasets. The cluster centres have zero, one, or two significant off-diagonal points, representing zero, one, or two holes in the datasets.

as m . To compute the weighted Fréchet mean, we need to find $\mathbb{M}_k = \{y^{(i)}\}_{i=1}^m$ that minimises the Fréchet function in (2). Implicit to the Wasserstein distance is a bijection $\gamma_j : y^{(i)} \mapsto x_j^{(i)}$ for each j . Supposing we know these bijections, we can rearrange the Fréchet function into the form $F(\mathbb{M}_k) = \sum_{j=1}^n r_{jk}^2 W_2(\mathbb{M}_k, \mathbb{D}_j)^2 = \sum_{i=1}^m \sum_{j=1}^n r_{jk}^2 \|y^{(i)} - x_j^{(i)}\|^2$.

In this form, the summand is minimised for $y^{(i)}$ by the weighted Euclidean centroid of the points $\{x_j^{(i)}\}_{j=1}^n$. Therefore to compute the weighted Fréchet mean, we need to find the correct bijections. We start by using the Hungarian algorithm to find an optimal matching between \mathbb{M}_k and each \mathbb{D}_j . Given a \mathbb{D}_j , for each point $y^{(i)} \in \mathbb{M}_k$, the Hungarian algorithm will assign an optimally matched point $x_j^{(i)} \in \mathbb{D}_j$. Specifically, we find matched points

$$\left[x_j^{(i)} \right]_{i=1}^m \leftarrow \text{Hungarian}(\mathbb{M}_k, \mathbb{D}_j), \text{ for each } j = 1, \dots, n. \quad (3)$$

Now, for each $y^{(i)} \in \mathbb{M}_k$ we need to find the weighted average of the matched points $\left[x_j^{(i)} \right]_{j=1}^n$. However, some of these points could be copies of the diagonal, so we need to consider three distinct cases: that each matched point is off-diagonal, that each one is a copy of the diagonal, or that the points are a mixture of both. We start by partitioning $1, \dots, n$ into the indices of the off-diagonal points $\mathcal{J}_{\text{OD}}^{(i)} = \{j : x_j^{(i)} \neq \Delta\}$ and the indices of the diagonal points $\mathcal{J}_{\Delta}^{(i)} = \{j : x_j^{(i)} = \Delta\}$ for each $i = 1, \dots, m$. Now, if $\mathcal{J}_{\text{OD}} = \emptyset$ then $y^{(i)}$ is a copy of the diagonal. If not, let $w = \left(\sum_{j \in \mathcal{J}_{\text{OD}}^{(i)}} r_{jk}^2 \right)^{-1} \sum_{j \in \mathcal{J}_{\text{OD}}^{(i)}} r_{jk}^2 x_j^{(i)}$ be the weighted mean of the off-diagonal points. If $\mathcal{J}_{\Delta}^{(i)} = \emptyset$, then $y^{(i)} = w$. Otherwise, let w_{Δ} be the point on the diagonal closest to w . Then our update is

$$y^{(i)} \leftarrow \frac{\sum_{j \in \mathcal{J}_{\text{OD}}^{(i)}} r_{jk}^2 x_j^{(i)} + \sum_{j \in \mathcal{J}_{\Delta}^{(i)}} r_{jk}^2 w_{\Delta}}{\sum_{j=1}^n r_{jk}^2}, \text{ for } i = 1, \dots, m. \quad (4)$$

We alternate between (3) and (4) until the matching remains the same. Theorem 2, proving that this algorithm converges to a local minimum of the Fréchet function, is proven in Appendix B. Also in Appendix B is Algorithm 2, giving an overview of the entire computation.

Theorem 2. *Given diagrams \mathbb{D}_j , membership values r_{jk} , and the Fréchet function $F(\hat{\mathbb{D}}) = \sum_{j=1}^n r_{jk}^2 W_2(\hat{\mathbb{D}}, \mathbb{D}_j)^2$, then $\mathbb{M}_k = \{y^{(i)}\}_{i=1}^m$ is a local minimum of F if and only if there is a unique optimal pairing from \mathbb{M}_k to each of the \mathbb{D}_j and each $y^{(i)}$ is updated via (4).*

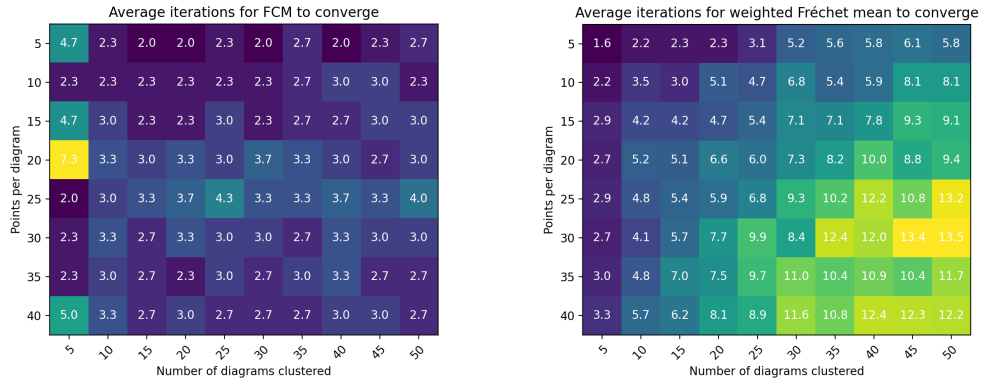


Figure 3: Heatmaps showing average number of iterations for fuzzy clustering of persistence diagrams (left) and the weighted Fréchet mean computation (right) to converge. Convergence of the FCM algorithm is determined when the cost function is stable to within $\pm 0.5\%$. Convergence experiments were carried out on randomly generated persistence diagrams with three repeats.

4 EXPERIMENTS

4.1 SYNTHETIC DATA

Exemplar clustering. We start by demonstrating our algorithm on a simple synthetic dataset designed to highlight its ability to cluster based on the topology of the underlying datasets. We produce three datasets of noise, three datasets of a ring, and three datasets of figure-of-eights, all shown in Figure 2(a). In Figure 2(b) we show the corresponding 1-PH persistence diagrams. Note that the persistence diagrams have either zero, one, or two significant off-diagonal points, corresponding to zero, one, or two holes in the datasets. We then use our algorithm to cluster the nine persistence diagrams into three clusters. Having only been given the list of diagrams, the number of clusters, and the maximum number of iterations, our algorithm successfully clusters the diagrams based on their topology. Figure 2(c) shows that the cluster centres have zero, one, or two off-diagonal points: our algorithm has found cluster centres that reflect the topological features of the datasets. Because we are reducing the cardinality and dimensionality of datasets by mapping into persistence diagrams, we also demonstrate a speed-up of at least an order of magnitude over Wasserstein barycentre clustering methods. Details of these timing experiments are in Appendix C.1.³

Empirical behaviour. Figure 4 shows the results of experiments run to determine the empirical performance of our algorithm. We give theoretical guarantees that every convergent subsequence will tend to a local minimum, but in practice it remains important that our algorithm will converge, and within a reasonable timeframe. To this end we ran experiments on a total of 825 randomly generated persistence diagrams, recording the number of iterations and cost functions for both the FCM clustering and the weighted Fréchet mean (WFM) computation. We considered the FCM to have converged when the cost function remained within $\pm 0.5\%$. As explained in Section 3.2, the WFM converges when the matching stays the same. Our experiments showed that the FCM clustering consistently converges within <5 iterations, regardless of the number of diagrams and points per diagram (note that the *time per iteration* increases as the number of points/diagrams increases, even if the number of iterations remains stable). We had no experiments in which the algorithm did not converge. The WFM computation requires more iterations as both number of diagrams and number of points per diagram increases, but we once again experienced no failures to converge in each of our experiments. In general, running the algorithm offered no difficulties on a laptop, and we believe the algorithm is ready for use by practitioners in the TDA community.

³Further details of all experiments are available in Appendix C.

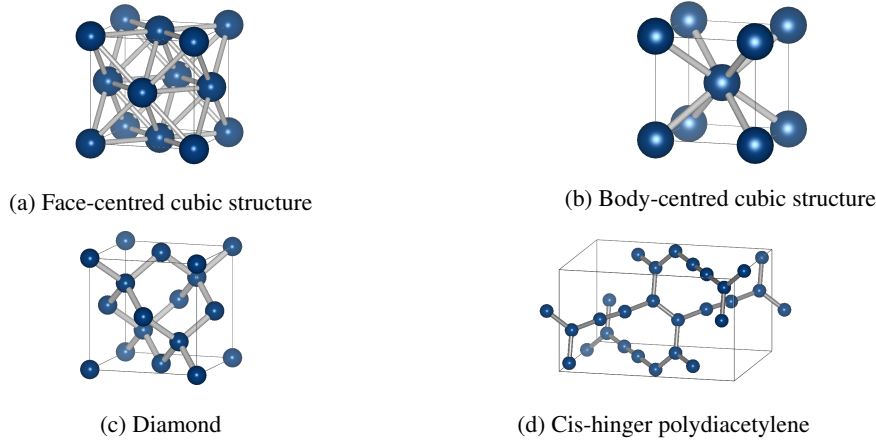


Figure 4: Cubic structures (top) and carbon allotropes (bottom). Our algorithm can cluster transformed lattice structures where comparable geometric algorithms fail.

4.2 LATTICE STRUCTURES

A key property for machine learning in materials science has been identified as “invariance to the basis symmetries of physics [...] rotation, reflection, translation” (Schmidt et al., 2019). Removing the need for a standardised coordinate system allows machine learning methods to be applied to a broader range of existing coordinate datasets generated by experimental methods (e.g., x-ray diffraction and scanning electron microscope imaging) and computational methods (e.g., density functional theory). Persistence diagrams, which capture affine transformation-invariant properties of datasets, are ideally suited for application in this domain. Our algorithm enables successful unsupervised learning on these datasets for the first time. Additionally, the fuzzy membership values allow top- k ranking of candidates suggested by our algorithm. This is particularly important in materials science, where further investigation of materials can be extremely costly.

The large majority of solids are comprised of lattices: regularly repeating unit cells of atoms. This lattice structure directly determines the properties of a material (Hull & Bacon, 2011) and it has been predicted that machine learning will reveal presently unknown links between structure and property by identifying new trends across materials (Meredig, 2019; Wei et al., 2019). We apply our algorithm to two examples of lattice structures from materials science: cubic structures and carbon allotropes. Cubic structures are important because they are ubiquitous. The most common lattice structures, particularly amongst pure metals, are face-centred cubic (FCC) structures and body-centred cubic (BCC) structures (Putnis, 1992), shown in Figures 4(a) and 4(b). Carbon allotropes, such as graphene and diamond, are widely anticipated to revolutionise electronics and optoelectronics (Wang et al., 2016). We focus on the carbon allotropes diamond and cis-hinged polydiacetylene, shown in Figures 4(c) and 4(d).

We use atomic positions for the unit-cells of iron mp-150 and iron mp-13 from the Materials Project (Jain et al., 2013), representing BCC and FCC structures respectively, for our first experiment. For our second experiment we use diamond and cis-hinged polydiacetylene unit-cell atomic positions from the Samara Carbon Allotrope Database (Hoffmann et al., 2016). We simulate distinct collections of lattices by transforming the atomic coordinates, with no information about bonds given to the algorithms. The properties of persistence diagrams mean that we can successfully cluster the atomic coordinates derived from the same base unit-cell regardless of the transformations applied to the coordinate system, fulfilling the key property identified above (we consider a clustering successful when all datasets from the same lattice structure have their highest membership values for the same cluster). In comparison, we run Wasserstein barycentre clustering on the same datasets using several state-of-the-art algorithms for barycentre computation and approximation. Each can only successfully cluster the cubic structures after reflection, and none of them successfully cluster the carbon allotropes after any transformations. We give specific values for these results in Appendix C.2.

4.3 DECISION BOUNDARIES

Learnt models have been shown to perform better on datasets which have a similar persistence diagram to the model’s decision boundary (Ramamurthy et al., 2019). In fact, topological complexity has been shown to correlate with generalisation ability (Guss & Salakhutdinov, 2018; Gabrielsson & Carlsson, 2019; Rieck et al., 2018). We utilise our algorithm to cluster the topology of models and tasks, showing that high membership values imply better performance on tasks. Specifically, given a dataset with n classes, we fix one class to define $n - 1$ tasks: binary classification of the fixed class vs each of the remaining classes. On each of these tasks, we train a *model*. We compute the decision boundary of the model f , defined as $(x_1, \dots, x_m, f(x))$ where $f(x)$ is the model’s prediction for $x = (x_i)_i$, and the decision boundary of the tasks, defined via the labelled dataset as (x_1, \dots, x_m, y) where y is the true label. We compute the 1-persistence diagrams of the tasks’ and models’ decision boundaries and cluster them to obtain membership values and cluster centres. To view task and model proximity through our clustering, we find the cluster centre with the highest membership value for each task, and consider the models closest to that cluster centre. Note that in general you cannot do this with hard clustering: most of the time a path will not exist from task to cluster centre to model, because each task/model is only associated with a single cluster. This contrasts with fuzzy clustering, where you have information about how close each model/task is to each cluster centre. We further discuss why this does not work for hard clustering in Appendix C.3.

To assess the ability of our model/task clustering, we performed the above experiment on three different datasets: MNIST (LeCun et al., 2010), FashionMNIST (Xiao et al., 2017), and Kuzushiji-MNIST (Clanuwat et al., 2018). We repeat each experiment three times. Our goal is to evaluate whether or not the clustering is capturing information about model performance on tasks, so as a baseline we use the average performance of all models on a fixed task, averaged over all tasks. Recall that we are just using the topology of the decision boundary: no information about model performance on the task was used until we assessed the ability of the clustering to capture information about the tasks. We start by verifying what happens if we use the model closest to the cluster centre associated with the task (i.e., top-1). We see a significant increase in performance, indicating that the topological fuzzy clustering has selected the model trained on the task: this means the clustering is working. We also compute the top-3 and top-2 performance change over average. We still see a statistically significant increase in performance over average performance, indicating that our membership values are capturing information about model performance on unseen tasks. These results are shown in Table 1. By successfully matching models to tasks using fuzzy clustering, we offer a new technique for future model marketplaces, demonstrating the value of topological clustering when analysing decision boundaries.

Table 1: Performance increase/decrease over average task performance when using learnt fuzzy membership values for model selection. The increase in performance demonstrates that our fuzzy clustering automatically clusters models near tasks they perform well on.

	Performance change vs random model selection (%)		
	Top-3	Top-2	Top-1
MNIST	$+6.17^{\pm 2.18}$	$+10.81^{\pm 1.88}$	$+20.88^{\pm 4.08}$
FashionMNIST	$+16.46^{\pm 4.00}$	$+21.94^{\pm 4.73}$	$+23.30^{\pm 8.72}$
Kuzushiji	$+6.61^{\pm 1.78}$	$+11.18^{\pm 2.45}$	$+21.89^{\pm 5.54}$

5 CONCLUSIONS

We have developed FCM clustering on the space of persistence diagrams, adding an important class of unsupervised learning to Topological Data Analysis’ toolkit. Our topological fuzzy clustering paves the way for applications in materials science and pre-trained model marketplaces, where we envisage our algorithm being used as part of automated materials discovery and model selection.

REFERENCES

Ulrich Bauer. Ripser: efficient computation of vietoris-rips persistence barcodes, August 2019. Preprint.

Jean-David Benamou, Guillaume Carlier, Marco Cuturi, Luca Nenna, and Gabriel Peyré. Iterative bregman projections for regularized transportation problems. *SIAM Journal on Scientific Computing*, 2015. doi: 10.1137/141000439.

J. C. Bezdek. A convergence theorem for the fuzzy isodata clustering algorithms. *IEEE Transactions on Pattern Analysis and Machine Intelligence*, PAMI-2(1):1–8, Jan 1980. ISSN 1939-3539. doi: 10.1109/TPAMI.1980.4766964.

J. C. Bezdek, R. J. Hathaway, M. J. Sabin, and W. T. Tucker. Convergence theory for fuzzy c-means: Counterexamples and repairs. *IEEE Transactions on Systems, Man, and Cybernetics*, 17(5):873–877, 1987.

Peter Bubenik. Statistical topological data analysis using persistence landscapes. *Journal of Machine Learning Research*, 16(3):77–102, 2015. URL <http://jmlr.org/papers/v16/bubenik15a.html>.

Peter Bubenik and Alexander Wagner. Embeddings of persistence diagrams into hilbert spaces. *CoRR*, abs/1905.05604, 2019. URL <http://arxiv.org/abs/1905.05604>.

Mathieu Carrière and Ulrich Bauer. On the metric distortion of embedding persistence diagrams into separable hilbert spaces. In *Symposium on Computational Geometry*, 2019.

Mathieu Carrière, Marco Cuturi, and S. Oudot. Sliced wasserstein kernel for persistence diagrams. In *ICML*, 2017.

Mathieu Carrière, Frédéric Chazal, Yuichi Ike, T. Lacombe, Martin Royer, and Y. Umeda. Perslay: A neural network layer for persistence diagrams and new graph topological signatures. In *AISTATS*, 2020.

Frédéric Chazal, Vin Silva, Marc Glisse, and Steve Oudot. *The Structure and Stability of Persistence Modules*. 07 2012. doi: 10.1007/978-3-319-42545-0.

Chao Chen, Xiuyan Ni, Qinxun Bai, and Yusu Wang. Toporeg: A topological regularizer for classifiers. *CoRR*, abs/1806.10714, 2018. URL <http://arxiv.org/abs/1806.10714>.

Sofya Chepushtanova, Tegan Emerson, Eric Hanson, Michael Kirby, Francis Motta, Rachel Neville, Chris Peterson, Patrick Shipman, and Lori Ziegelmeier. Persistence images: An alternative persistent homology representation. 07 2015.

Tarin Clanuwat, Mikel Bober-Irizar, Asanobu Kitamoto, Alex Lamb, Kazuaki Yamamoto, and David Ha. Deep learning for classical japanese literature, 2018.

J. Clough, N. Byrne, I. Oksuz, V. A. Zimmer, J. A. Schnabel, and A. King. A topological loss function for deep-learning based image segmentation using persistent homology. *IEEE Transactions on Pattern Analysis and Machine Intelligence*, pp. 1–1, 2020.

David Cohen-Steiner, Herbert Edelsbrunner, and John Harer. Stability of persistence diagrams. *Discrete & Computational Geometry*, 37(1):103–120, Jan 2007. ISSN 1432-0444. doi: 10.1007/s00454-006-1276-5. URL <https://doi.org/10.1007/s00454-006-1276-5>.

David Cohen-Steiner, Herbert Edelsbrunner, and John Harer. Extending persistence using poincare and lefschetz duality. *FOUNDATIONS OF COMPUTATIONAL MATHEMATICS*, pp. 2009, 2009.

Marco Cuturi and Arnaud Doucet. Fast computation of wasserstein barycenters. volume 32 of *Proceedings of Machine Learning Research*, pp. 685–693, Bejing, China, 22–24 Jun 2014. PMLR. URL <http://proceedings.mlr.press/v32/cuturi14.html>.

F. d. A. T. de Carvalho, A. Iripino, and R. Verde. Fuzzy clustering of distribution-valued data using an adaptive l_2 wasserstein distance. In *2015 IEEE International Conference on Fuzzy Systems (FUZZ-IEEE)*, pp. 1–8, 2015.

Herbert Edelsbrunner and John Harer. *Computational Topology - an Introduction*. American Mathematical Society, 2010. ISBN 978-0-8218-4925-5.

Herbert Edelsbrunner, David Letscher, and Afra Zomorodian. Topological persistence and simplification. volume 28, pp. 454 – 463, 02 2000. ISBN 0-7695-0850-2. doi: 10.1109/SFCS.2000.892133.

Barbara Di Fabio and Massimo Ferri. Comparing persistence diagrams through complex vectors. In *Image Analysis and Processing — ICIAP 2015*, pp. 294–305. Springer International Publishing, 2015. doi: 10.1007/978-3-319-23231-7_27. URL https://doi.org/10.1007/978-3-319-23231-7_27.

Rickard Brüel Gabrielsson and G. Carlsson. Exposition and interpretation of the topology of neural networks. *2019 18th IEEE International Conference On Machine Learning And Applications (ICMLA)*, pp. 1069–1076, 2019.

Rickard Brüel Gabrielsson, Bradley J. Nelson, Anjan Dwaraknath, and Primoz Skraba. A topology layer for machine learning. volume 108 of *Proceedings of Machine Learning Research*, pp. 1553–1563, Online, 26–28 Aug 2020. PMLR. URL <http://proceedings.mlr.press/v108/gabrielsson20a.html>.

Marian Gidea and Yuri Katz. Topological data analysis of financial time series: Landscapes of crashes. *Physica A: Statistical Mechanics and its Applications*, 491:820–834, February 2018. doi: 10.1016/j.physa.2017.09.028. URL <https://doi.org/10.1016/j.physa.2017.09.028>.

William H. Guss and R. Salakhutdinov. On characterizing the capacity of neural networks using algebraic topology. *ArXiv*, abs/1802.04443, 2018.

Christoph Hofer, Roland Kwitt, Marc Niethammer, and Andreas Uhl. Deep learning with topological signatures. In I. Guyon, U. V. Luxburg, S. Bengio, H. Wallach, R. Fergus, S. Vishwanathan, and R. Garnett (eds.), *Advances in Neural Information Processing Systems 30*, pp. 1634–1644. Curran Associates, Inc., 2017. URL <http://papers.nips.cc/paper/6761-deep-learning-with-topological-signatures.pdf>.

Roald Hoffmann, Artem Kabanov, Andrey Golov, and Davide Proserpio. Homo citans and carbon allotropes: For an ethics of citation. *Angewandte Chemie International Edition*, 55, 07 2016. doi: 10.1002/anie.201600655.

D. Hull and D.J. Bacon. *Introduction to Dislocations (Fifth Edition)*. Butterworth-Heinemann, Oxford, fifth edition edition, 2011. ISBN 978-0-08-096672-4. doi: <https://doi.org/10.1016/B978-0-08-096672-4.00019-0>. URL <http://www.sciencedirect.com/science/article/pii/B9780080966724000190>.

Anubhav Jain, Shyue Ping Ong, Geoffroy Hautier, Wei Chen, William Davidson Richards, Stephen Dacek, Shreyas Cholia, Dan Gunter, David Skinner, Gerbrand Ceder, and Kristin a. Persson. The Materials Project: A materials genome approach to accelerating materials innovation. *APL Materials*, 1(1):011002, 2013. ISSN 2166532X. doi: 10.1063/1.4812323. URL <http://link.aip.org/link/AMPADS/v1/i1/p011002/s1&Agg=doi>.

Sara Kališnik. Tropical coordinates on the space of persistence barcodes. *Foundations of Computational Mathematics*, 19(1):101–129, January 2018. doi: 10.1007/s10208-018-9379-y. URL <https://doi.org/10.1007/s10208-018-9379-y>.

Michael Kerber, Dmitriy Morozov, and Arnur Nigmetov. Geometry helps to compare persistence diagrams. *Journal of Experimental Algorithmics (JEA)*, 22:1–20, 2017.

Kwangho Kim, Jisu Kim, J. Kim, Frédéric Chazal, and L. Wasserman. Efficient topological layer based on persistent landscapes. *ArXiv*, abs/2002.02778, 2020.

Frank Klawonn. Fuzzy clustering: Insights and a new approach. *Mathware & soft computing*, ISSN 1134-5632, Vol. 11, N°. 3, 2004, pags. 125-142, 11, 01 2004.

Violeta Kovacev-Nikolic, Peter Bubenik, Dragan Nikolić, and Giseon Heo. Using persistent homology and dynamical distances to analyze protein binding. *Statistical Applications in Genetics and Molecular Biology*. January 2016, Volume 15, Issue 1, Pages 19-38, 2014.

Theo Lacombe, Marco Cuturi, and Steve Oudot. Large scale computation of means and clusters for persistence diagrams using optimal transport. In S. Bengio, H. Wallach, H. Larochelle, K. Grauman, N. Cesa-Bianchi, and R. Garnett (eds.), *Advances in Neural Information Processing Systems 31*, pp. 9770–9780. Curran Associates, Inc., 2018.

Tam Le and Makoto Yamada. Persistence fisher kernel: A riemannian manifold kernel for persistence diagrams. In *NeurIPS*, 2018.

Yann LeCun, Corinna Cortes, and CJ Burges. Mnist handwritten digit database. *ATT Labs [Online]*. Available: <http://yann.lecun.com/exdb/mnist>, 2, 2010.

J. Li and J. Z. Wang. Real-time computerized annotation of pictures. *IEEE Transactions on Pattern Analysis and Machine Intelligence*, 30(6):985–1002, 2008.

H. Ling and K. Okada. An efficient earth mover’s distance algorithm for robust histogram comparison. *IEEE Transactions on Pattern Analysis and Machine Intelligence*, 29(5):840–853, 2007.

Vasileios Maroulas, Joshua Mike, and Andrew Marchese. K-means clustering on the space of persistence diagrams. In *SPIE*, pp. 29, 08 2017. doi: 10.1117/12.2273067.

Bryce Meredig. Five high-impact research areas in machine learning for materials science. *Chemistry of Materials*, 31(23):9579–9581, 2019. doi: 10.1021/acs.chemmater.9b04078. URL <https://doi.org/10.1021/acs.chemmater.9b04078>.

Yuriy Mileyko, Sayan Mukherjee, and John Harer. Probability measures on the space of persistence diagrams. *Inverse Problems - INVERSE PROBL*, 27, 12 2011. doi: 10.1088/0266-5611/27/12/124007.

M. Moor, Max Horn, Bastian Alexander Rieck, and K. Borgwardt. Topological autoencoders. *ArXiv*, abs/1906.00722, 2019.

Andrew Putnis. *An Introduction to Mineral Sciences*. Cambridge University Press, 1992. doi: 10.1017/CBO9781139170383.

Karthikeyan Natesan Ramamurthy, Kush Varshney, and Krishnan Mody. Topological data analysis of decision boundaries with application to model selection. volume 97 of *Proceedings of Machine Learning Research*, pp. 5351–5360, Long Beach, California, USA, 09–15 Jun 2019. PMLR. URL <http://proceedings.mlr.press/v97/ramamurthy19a.html>.

J. Reininghaus, S. Huber, U. Bauer, and R. Kwitt. A stable multi-scale kernel for topological machine learning. In *2015 IEEE Conference on Computer Vision and Pattern Recognition (CVPR)*, pp. 4741–4748, 2015.

Bastian Rieck, Matteo Togninalli, Christian Bock, Michael Moor, Max Horn, Thomas Gumsch, and Karsten M. Borgwardt. Neural persistence: A complexity measure for deep neural networks using algebraic topology. *CoRR*, abs/1812.09764, 2018. URL <http://arxiv.org/abs/1812.09764>.

Bastian Alexander Rieck, F. Sadlo, and H. Leitte. Topological machine learning with persistence indicator functions. *ArXiv*, abs/1907.13496, 2019.

Jonathan Schmidt, Mário R. G. Marques, Silvana Botti, and Miguel A. L. Marques. Recent advances and applications of machine learning in solid-state materials science. *npj Computational Materials*, 5(1):83, 2019. ISSN 2057-3960. doi: 10.1038/s41524-019-0221-0. URL <https://doi.org/10.1038/s41524-019-0221-0>.

Katharine Turner and Gard Spreemann. Same but different: Distance correlations between topological summaries. *arXiv: Algebraic Topology*, 2019.

Katharine Turner, Yuriy Mileyko, Sayan Mukherjee, and John Harer. Fréchet means for distributions of persistence diagrams. *Discrete & Computational Geometry*, 52:44–70, 2012.

J. Vidal, J. Budin, and J. Tierny. Progressive wasserstein barycenters of persistence diagrams. *IEEE Transactions on Visualization and Computer Graphics*, 26(1):151–161, 2020.

L. Vietoris. Über den höheren Zusammenhang kompakter Räume und eine Klasse von zusammenhangstreuen Abbildungen. *Mathematische Annalen*, 97(1):454–472, December 1927. doi: 10.1007/bf01447877. URL <https://doi.org/10.1007/bf01447877>.

Alexander Wagner. Nonembeddability of persistence diagrams with $p > 2$ Wasserstein metric. *ArXiv*, abs/1910.13935, 2019.

Zhanyu Wang, F. Dong, Bo Shen, R. Zhang, Y. Zheng, L. Chen, Songyou Wang, Chongmin Wang, K. Ho, Yuan-Jia Fan, Bih-Yaw Jin, and Wan-Sheng Su. Electronic and optical properties of novel carbon allotropes. *Carbon*, 101:77–85, 01 2016. doi: 10.1016/j.carbon.2016.01.078.

Jing Wei, Xuan Chu, Xiang-Yu Sun, Kun Xu, Hui-Xiong Deng, Jigen Chen, Zhongming Wei, and Ming Lei. Machine learning in materials science. *InfoMat*, 1:338–358, 09 2019. doi: 10.1002/inf2.12028.

B. Wilder, Eric Ewing, B. Dilkina, and Milind Tambe. End to end learning and optimization on graphs. In *NeurIPS*, 2019.

Han Xiao, Kashif Rasul, and Roland Vollgraf. Fashion-mnist: a novel image dataset for benchmarking machine learning algorithms, 2017.

J. Ye and J. Li. Scaling up discrete distribution clustering using admm. In *2014 IEEE International Conference on Image Processing (ICIP)*, pp. 5267–5271, 2014.

Jianbo Ye, Panruo Wu, James Wang, and Jia Li. Fast discrete distribution clustering using Wasserstein barycenter with sparse support. *IEEE Transactions on Signal Processing*, PP:1–1, 01 2017. doi: 10.1109/TSP.2017.2659647.

W.I. Zangwill. *Nonlinear programming: a unified approach*. Prentice-Hall International Series in management. Prentice-Hall, 1969. URL <https://books.google.co.uk/books?id=TWhxLcApH9sC>.

Qi Zhao and Yusu Wang. Learning metrics for persistence-based summaries and applications for graph classification. In H. Wallach, H. Larochelle, A. Beygelzimer, F. d’Alché-Buc, E. Fox, and R. Garnett (eds.), *Advances in Neural Information Processing Systems 32*, pp. 9859–9870. Curran Associates, Inc., 2019.

Bartosz Zieliński, Michał Lipiński, Mateusz Juda, Matthias Zeppelzauer, and Paweł Dłotko. Persistence bag-of-words for topological data analysis. In *Proceedings of the Twenty-Eighth International Joint Conference on Artificial Intelligence, IJCAI-19*, pp. 4489–4495. International Joint Conferences on Artificial Intelligence Organization, 7 2019. doi: 10.24963/ijcai.2019/624. URL <https://doi.org/10.24963/ijcai.2019/624>.

Afra Zomorodian and Gunnar Carlsson. Computing Persistent Homology. *Discrete & Computational Geometry*, 33(2):249–274, 2005. ISSN 1432-0444. doi: 10.1007/s00454-004-1146-y. URL <https://doi.org/10.1007/s00454-004-1146-y>.

A CONVERGENCE OF THE FCM CLUSTERING ALGORITHM

We first need to consider our separate updates as a single update procedure. Let $F : \mathbb{M} \mapsto R$ be defined by (1) and $G : R \mapsto \mathbb{M}$ be defined by (2), and for $R = \{r_{jk}\}$ and $\mathbb{M} = \{\mathbb{M}_k\}$ consider the sequence

$$\left\{ T^{(l)}(R, \mathbb{M}) : l = 0, 1, \dots \right\}, \text{ where } T(R, M) = (F \circ G(R), G(R)).$$

We wish to show convergence of the iterates of T to a local minimum or saddle point of the cost function

$$J(R, \mathbb{M}) = \sum_{j=1}^n \sum_{k=1}^c r_{jk}^2 W_2(\mathbb{M}_k, \mathbb{D}_j)^2.$$

The two stage update process of T is too complicated to use standard fixed point theorems, so as in Bezdek (1980) we shall use the following result, which is proven in Zangwill (1969).

Theorem 3 (Zangwill's Convergence Theorem). *Let $A : X \rightarrow 2^X$ be a point-to-set algorithm acting on X . Given $x_0 \in X$, generate a sequence $\{x_k\}_{k=1}^\infty$ such that $x_{k+1} \in A(x_k)$ for every k . Let $\Gamma \subset X$ be a solution set, and suppose that the following hold.*

- (i) *The sequence $\{x_k\} \subset S \subset X$ for a compact set S .*
- (ii) *There exists a continuous function Z on X such that if $x \notin \Gamma$ then $Z(y) < Z(x)$ for all $y \in A(x)$, and if $x \in \Gamma$ then $Z(y) \leq Z(x)$ for all $y \in A(x)$. The function Z is called a descent function.*
- (iii) *The algorithm A is closed on $X \setminus \Gamma$.*

Then every convergent subsequence of $\{x_k\}$ tends to a point in the solution set Γ .

Our algorithm is the update function T . We define our solution set as

$$\Gamma = \left\{ (R, \mathbb{M}) : J(R, \mathbb{M}) < J(\hat{R}, \hat{\mathbb{M}}) \forall (\hat{R}, \hat{\mathbb{M}}) \in B((R, \mathbb{M}), r) \right\}$$

for some $r > 0$, where the ball surrounding R is the Euclidean ball in \mathbb{R}^{nc} and the ball surrounding \mathbb{M} is $\cup_{k=1}^c B_{W_2}(\mathbb{M}_k, r)$. This set contains the local minima and saddle points of the cost function (Bezdek et al., 1987). We wish to show that our cost function $J(R, \mathbb{M})$ is the descent function Z . We proceed by verifying each of the requirements for Zangwill's Convergence Theorem.

Lemma 4. *Every iterate $T^{(l)}(R, \mathbb{M}) \in [0, 1]^{nc} \times \text{conv}(\mathbb{D})^c$, where*

$$\text{conv}(\mathbb{D}) = \bigcup_{k=1}^c \bigcup_{\gamma_j} \bigcup_{i=1}^m \text{conv}\{\gamma_j(y^{(i)}) : j = 1, \dots, n\},$$

with γ_j a bijection $\mathbb{M}_k \rightarrow \mathbb{D}_j$ and $\text{conv}\{\gamma_j(y^{(i)}) : j = 1, \dots, n\}$ the ordinary convex hull in the plane. Furthermore, $[0, 1]^{nc} \times \text{conv}(\mathbb{D})^c$ is compact.

Proof. By construction, every $r_{jk} \in [0, 1]$. Since $j = 1, \dots, n$ and $k = 1, \dots, c$, we can view R as a point in $[0, 1]^{nc}$, and so every iterate of R is in $[0, 1]^{nc}$. We shall show that for a fixed k and a fixed bijection $\gamma_j : \mathbb{M}_k \rightarrow \mathbb{D}_j$, each updated $y^{(i)}$ is contained in a convex combination of $\{\gamma_j(y^{(i)}) : j = 1, \dots, n\}$. Where $\gamma_j(y^{(i)}) = \Delta$, let $\gamma_j(y^{(i)}) = w_\Delta$ as defined in (4), as this is the update point we use for the diagonal. Since there are a finite number of off-diagonal points, each updated \mathbb{M}_k is therefore contained in the union over all bijections and all points $y^{(i)}$ of the convex combination of $\{\gamma_j(y^{(i)}) : j = 1, \dots, n\}$. By also taking the union over each k , we show that every iterate of \mathbb{M} must be contained in the finite triple-union of the convex combination of each possible bijection. To show that each updated $y^{(i)}$ is contained in a convex combination of $\{\gamma_j(y^{(i)}) : j = 1, \dots, n\}$, recall that $y^{(i)} = \left(\sum_{j=1}^n r_{jk}^2\right)^{-1} \sum_{j=1}^n r_{jk}^2 \gamma_j(y^{(i)})$. Letting $t_j^{(i)} = r_{jk}^2 \left(\sum_{j=1}^n r_{jk}^2\right)^{-1}$, clearly each $t_j^{(i)} > 0$ and $\sum_{j=1}^n t_j^{(i)} = 1$. Since $y^{(i)} = \sum_{j=1}^n t_j^{(i)} \gamma_j(y^{(i)})$, each $y^{(i)}$ is contained in the convex combination. Therefore $T^{(l)}(R, \mathbb{M}) \in [0, 1]^{nc} \times \text{conv}(\mathbb{D})^c$ for each $l = 0, 1, \dots$.

Now, $[0, 1]$ is closed and bounded, so is compact. The convex hull of points in the plane is closed and bounded, so $\text{conv}\{\gamma_j(y^{(i)}) : j = 1, \dots, n\}$ is compact. Since finite unions and finite direct products of compact sets are compact, $[0, 1]^{nc} \times \text{conv}(\mathbb{D})^c$ is also compact. \square

Lemma 5. *The cost function $J(R, \mathbb{M})$ is a descent function, as defined in Theorem 3(ii).*

Proof. The cost function J is continuous, as it's a sum, product and composition of continuous functions. Furthermore, we have that for any $(R, \mathbb{M}) \notin \Gamma$,

$$J(T(R, \mathbb{M})) = J(F \circ G(R), G(R)) < J(R, G(R)) < J(R, M),$$

where the first inequality is due to Proposition 1 in Bezdek (1980), and the second inequality comes from the definition of the Fréchet mean. If $(R, \mathbb{M}) \in \Gamma$ then the strict inequalities include equality throughout. \square

Theorem 6. *For any (R, \mathbb{M}) , every convergent subsequence of $\{T^{(l)}(R, \mathbb{M}) : l = 0, 1, \dots\}$ tends to a local minimum or saddle point of the cost function J .*

Proof. We proceed with Zangwill's Convergence Theorem. Our algorithm is the update function T , our solution set is Γ , and our descent function is the cost function $J(R, \mathbb{M})$. By Lemma 4, every iterate is contained within a compact set. By Lemma 5, J is a descent function. Finally, since our function T only maps points in the plane to points in the plane, it is a closed map. The theorem follows by applying Theorem 3. \square

B CONVERGENCE OF THE FRÉCHET MEAN ALGORITHM

Recall that the Fréchet mean is computed by finding the $\arg \min$ of

$$F(\hat{\mathbb{D}}) = \sum_{j=1}^n r_{jk}^2 F_j(\hat{\mathbb{D}}), \text{ with } F_j(\hat{\mathbb{D}}) = W_2(\hat{\mathbb{D}}, \mathbb{D}_j)^2, \quad (5)$$

for fixed k . We start by recounting work in Turner et al. (2012), which this section adapts for the weighted Fréchet mean.⁴ The proofs we're adapting use a gradient descent technique to prove local convergence. In order to use their techniques, we need to define a differential structure on the space of persistence diagrams.

By Theorem 2.5 in Turner et al. (2012), the space of persistence diagrams $\mathcal{D}_{L^2} = \{\mathbb{D} : W_2(\mathbb{D}, \Delta) < \infty\}$ is a non-negatively curved Alexandrov space. An optimal bijection $\gamma : \mathbb{D}_1 \rightarrow \mathbb{D}_2$ induces a unit-speed geodesic $\phi(t) = \{(1-t)x + t\gamma(x) : x \in \mathbb{D}_1, 0 \leq t \leq 1\}$. For a point $\mathbb{D} \in \mathcal{D}_{L^2}$ we define the tangent cone $T_{\mathbb{D}}$. Define $\hat{\Sigma}_{\mathbb{D}}$ as the set of all non-trivial unit-speed geodesics emanating from \mathbb{D} . Let $\phi, \eta \in \hat{\Sigma}_{\mathbb{D}}$ and define the angle between them as

$$\angle_{\mathbb{D}}(\phi, \eta) = \arccos \left(\lim_{s, t \downarrow 0} \frac{s^2 + t^2 - W_2(\phi(s), \eta(t))^2}{2st} \right) \in [0, \pi]$$

when the limit exists. Then the space of directions $(\Sigma_{\mathbb{D}}, \angle_{\mathbb{D}})$ is the completion of $\hat{\Sigma}_{\mathbb{D}} / \sim$ with respect to $\angle_{\mathbb{D}}$, with $\phi \sim \eta \iff \angle_{\mathbb{D}}(\phi, \eta) = 0$. We now define the tangent cone as

$$T_{\mathbb{D}} = (\Sigma_{\mathbb{D}} \times [0, \infty)) / (\Sigma_{\mathbb{D}} \times \{0\}).$$

Given $u = (\phi, s), v = (\eta, t)$, we define an inner product on the tangent cone by

$$\langle u, v \rangle = st \cos \angle_{\mathbb{D}}(\phi, \eta).$$

Now, for $\alpha > 0$ denote the space $(\mathcal{D}_{L^2}, \alpha W_2)$ as $\alpha \mathcal{D}_{L^2}$ and define the map $i_{\alpha} : \alpha \mathcal{D}_{L^2} \rightarrow \mathcal{D}_{L^2}$. For an open set $\Omega \subset \mathcal{D}_{L^2}$ and a function $f : \Omega \rightarrow \mathbb{R}$, the differential of f at $\mathbb{D} \in \Omega$ is defined by $d_{\mathbb{D}} f = \lim_{\alpha \rightarrow \infty} \alpha(f \circ i_{\alpha} - f(\mathbb{D}))$. Finally, we say that $s \in T_{\mathbb{D}}$ is a supporting vector of f at \mathbb{D} if $d_{\mathbb{D}} f(x) \leq -\langle s, x \rangle$ for all $x \in T_{\mathbb{D}}$.

⁴In Turner et al. (2012), the Fréchet mean is defined as the $\arg \min$ of the Fréchet function $F(\hat{\mathbb{D}}) = \int W_2(\hat{\mathbb{D}}, \mathbb{D}_j)^2 d\rho(\hat{\mathbb{D}})$ with the empirical measure $\rho = n^{-1} \sum_{j=1}^n \delta_{\mathbb{D}_j}$. We are using the empirical measure $\rho = \left(\sum_{j=1}^n r_{jk}^2 \right)^{-1} \sum_{j=1}^n r_{jk}^2 \delta_{\mathbb{D}_j}$, but for ease we drop the scalar $\left(\sum_{j=1}^n r_{jk}^2 \right)^{-1}$ as it is positive, so it does not affect the minimum of the function.

Lemma 7. *The following two results are proven in Turner et al. (2012).*

- (i) *Let $\mathbb{D} \in \mathcal{D}_{L^2}$. Let $F_j(\hat{\mathbb{D}}) = W_2(\hat{\mathbb{D}}, \mathbb{D}_j)^2$. Then if ϕ is a distance-achieving geodesic from \mathbb{D} to $\hat{\mathbb{D}}$, then the tangent vector to ϕ at \mathbb{D} of length $2W_2(\hat{\mathbb{D}}, \mathbb{D})$ is a supporting vector at \mathbb{D} of f .*
- (ii) *If \mathbb{D} is a local minimum of f and s is a supporting vector of f at \mathbb{D} , then $s = 0$.*

If there is a unique optimal matching $\gamma_{\mathbb{D}_1}^{\mathbb{D}_3} : \mathbb{D}_1 \rightarrow \mathbb{D}_3$, we say that it is induced by an optimal matching $\gamma_{\mathbb{D}_1}^{\mathbb{D}_2} : \mathbb{D}_1 \rightarrow \mathbb{D}_2$ if there exists a unique optimal matching $\gamma_{\mathbb{D}_2}^{\mathbb{D}_3} : \mathbb{D}_2 \rightarrow \mathbb{D}_3$ such that $\gamma_{\mathbb{D}_1}^{\mathbb{D}_3} = \gamma_{\mathbb{D}_2}^{\mathbb{D}_3} \circ \gamma_{\mathbb{D}_1}^{\mathbb{D}_2}$. Proposition 3.2 from Turner et al. (2012) states that an optimal matching at a point is also locally optimal. In particular, it states the following.

Lemma 8. *Let $\mathbb{D}_1, \mathbb{D}_2 \in \mathcal{D}_{L^2}$ such that there is a unique optimal matching from \mathbb{D}_1 to \mathbb{D}_2 . Then there exists an $r > 0$ such that for every $\mathbb{D}_3 \in B_{W_2}(\mathbb{D}_2, r)$, there is a unique optimal pairing from \mathbb{D}_2 to \mathbb{D}_3 that is induced by the matching from \mathbb{D}_1 to \mathbb{D}_2 .*

The following theorem proves that our algorithm converges to a local minimum of the Fréchet function.

Theorem 9. *Given diagrams \mathbb{D}_j , membership values r_{jk} , and the Fréchet function F defined in (5), then $\mathbb{M}_k = \{y^{(i)}\}_{i=1}^m$ is a local minimum of F if and only if there is a unique optimal pairing from \mathbb{M}_k to each of the \mathbb{D}_j , denoted γ_j , and each $y^{(i)}$ is updated via (4).*

Proof. First assume that γ_j are optimal pairings from \mathbb{M}_k to each \mathbb{D}_j , and let s_j be the vectors in $T_{\mathbb{M}_k}$ that are tangent to the geodesics induced by γ_j and are distance-achieving. Then by Lemma 7(i), each $2s_j$ is a supporting vector for the function F_j . Furthermore, $2 \sum_{j=1}^n r_{jk}^2 s_j$ is a supporting vector for F , as for any $\hat{\mathbb{D}}$,

$$\begin{aligned} d_{\mathbb{M}_k} F(\hat{\mathbb{D}}) &= d_{\mathbb{M}_k} \left(\sum_{j=1}^n r_{jk}^2 F_j(\hat{\mathbb{D}}) \right) = \sum_{j=1}^n r_{jk}^2 d_{\mathbb{M}_k} F_j(\hat{\mathbb{D}}) \\ &\leq \sum_{j=1}^n -r_{jk}^2 \langle 2s_j, \hat{\mathbb{D}} \rangle = - \left\langle 2 \sum_{j=1}^n r_{jk}^2 s_j, \hat{\mathbb{D}} \right\rangle. \end{aligned}$$

By Lemma 7(ii), $2 \sum_{j=1}^n r_{jk}^2 s_j = 0$. Putting $s_j = \gamma_j(y^{(i)}) - y^{(i)}$ and rearranging gives that $y^{(i)}$ updates via (4), as required. Note that when $\gamma_j(y^{(i)}) = \Delta$, we let $\gamma_j(y^{(i)}) = w_\Delta$ as defined in (4), because this minimises the transportation cost to the diagonal. Now suppose that γ_j and $\tilde{\gamma}_j$ are both optimal pairings. Then by the above argument $\sum_{j=1}^n r_{jk}^2 s_j = \sum_{j=1}^n r_{jk}^2 \tilde{s}_j = 0$, implying that $s_j = \tilde{s}_j$ and so $\gamma_j = \tilde{\gamma}_j$. Therefore the optimal pairing is unique.

To prove the opposite direction, assume that $\mathbb{M}_k = \{y^{(i)}\}$ locally minimises the Fréchet function F . Observe that for a fixed bijection γ_j , we have that

$$\begin{aligned} F(\mathbb{M}_k) &= \sum_{j=1}^n r_{jk}^2 W_2(\mathbb{M}_k, \mathbb{D}_j)^2 \\ &= \sum_{j=1}^n r_{jk}^2 \left(\inf_{\gamma_j : \hat{M} \rightarrow \mathbb{D}_j} \sum_{y \in \mathbb{M}_k} \|y - \gamma_j(y)\|^2 \right) \\ &= \sum_{j=1}^n r_{jk}^2 \sum_{i=1}^m \|y^{(i)} - x_j^{(i)}\|^2 \\ &= \sum_{i=1}^m \left(\sum_{j=1}^n r_{jk}^2 \|y^{(i)} - x_j^{(i)}\|^2 \right). \end{aligned}$$

The final term in brackets is non-negative, and minimised exactly when $y^{(i)}$ is updated via (4). Furthermore, the unique optimal pairing from \mathbb{M}_k to each of the \mathbb{D}_j 's is the same for every $\hat{\mathbb{M}}$ within the ball $B_{W_2}(\mathbb{M}_k, r)$ for some $r > 0$, by Lemma 8. Therefore, if \mathbb{M}_k is a local minimum of F , then the $y^{(i)}$'s are equal to the values found by taking the optimal pairings γ_j and calculating the weighted means of $\gamma_j(y^{(i)})$ with the weights r_{jk}^2 , as required. It will remain a minimum as long as the matching stays the same, which happens in the ball $B_{W_2}(\mathbb{M}_k, r)$, so we are done. \square

Algorithm 2 WFrechetMean

Input Diagrams $\mathbb{D} = \{\mathbb{D}_j\}_{j=1}^n$, Weights $R_k = \{r_{jk}\}_{j=1}^n$ (fixed k)
Output Weighted Fréchet mean $\mathbb{M}_k = \{y^{(i)}\}_{i=1}^m$

```

1:  $m \leftarrow \max_{1 \leq j \leq n} |\mathbb{D}_j|$ 
2: for  $j$  in  $1..n$  do
3:    $\left[ x_j^{(i)} \right]_{i=1}^m \leftarrow \text{HUNGARIAN}(\mathbb{M}_k, \mathbb{D}_j)$ 
4: end for
5: while  $\left\{ \left[ x_j^{(i)} \right]_{i=1}^m \right\}_{j=1}^n \neq \left\{ \left[ \hat{x}_j^{(i)} \right]_{i=1}^m \right\}_{j=1}^n$ 
   do
6:   for  $i$  in  $1..m$  do
7:      $\mathcal{J}_{\text{OD}}^{(i)} = \{j : x_j^{(i)} \neq \Delta\}$ 
8:      $\mathcal{J}_{\text{D}}^{(i)} = \{j : x_j^{(i)} = \Delta\}$ 
9:     if  $\mathcal{J}_{\text{OD}}^{(i)} = \emptyset$  then
10:     $y^{(i)} \leftarrow \Delta$ 
11:   else
12:      $w = \left( \sum_{j \in \mathcal{J}_{\text{OD}}^{(i)}} r_{jk}^2 \right)^{-1} \sum_{j \in \mathcal{J}_{\text{OD}}^{(i)}} r_{jk}^2 x_j^{(i)}$ 
13:     if  $\mathcal{J}_{\text{D}}^{(i)} = \emptyset$  then
14:        $y^{(i)} \leftarrow w$ 
15:     else
16:        $y^{(i)} \leftarrow \frac{\sum_{j \in \mathcal{J}_{\text{OD}}^{(i)}} r_{jk}^2 x_j^{(i)} + \sum_{j \in \mathcal{J}_{\text{D}}^{(i)}} r_{jk}^2 w_{\Delta}}{\sum_{j=1}^n r_{jk}^2}$ 
17:   end if
18: end if
19: end for
20:  $\left\{ \left[ \hat{x}_j^{(i)} \right]_{i=1}^m \right\}_{j=1}^n \leftarrow \left\{ \left[ x_j^{(i)} \right]_{i=1}^m \right\}_{j=1}^n$ 
21: for  $j$  in  $1..n$  do
22:    $\left[ x_j^{(i)} \right]_{i=1}^m \leftarrow \text{HUNGARIAN}(\mathbb{M}_k, \mathbb{D}_j)$ 
23: end for
24: end while
25: return  $\{y^{(i)}\}_{i=1}^m$ 

```

C EXPERIMENTAL DETAILS

C.1 SYNTHETIC DATA

Membership values. The membership values for the synthetic datasets are in Table 2. Datasets 1-3 are the datasets of noise, datasets 4-6 are the datasets with one ring, and datasets 7-9 are the datasets with two rings. We ran our algorithm for 20 iterations.

Table 2: Membership values for the synthetic dataset

Dataset	1	2	3	4	5	6	7	8	9
Cluster 1	0.6336	0.5730	0.5205	0.2760	0.2503	0.1974	0.2921	0.2128	0.2292
Cluster 2	0.1768	0.2057	0.2327	0.5361	0.5329	0.6371	0.2452	0.2291	0.1822
Cluster 3	0.1900	0.2212	0.2468	0.1879	0.2169	0.1655	0.4627	0.5580	0.5885

Timing experiments. For the timing experiments we divide the total number of points equally between four distributions, two of which are noise and two of which are shaped in a ring. Each clustering algorithm was run for five iterations on one core of a 2019 MacBook Pro with a 1.4GHz

Table 3: Seconds per clustering iteration

Points	100	200	300	400	500	600	700	800	900	1000
FPDCluster	0.01552	0.1975	0.9358	2.229	5.694	12.29	19.27	34.50	53.20	77.81
ADMM	5.622	34.86	161.3	617.6	-	-	-	-	-	-
BADMM	0.2020	2.188	26.38	112.6	-	-	-	-	-	-
SubGD	0.4217	2.273	22.17	103.4	-	-	-	-	-	-
IterBP	0.3825	2.226	21.57	108.9	-	-	-	-	-	-
LP	0.3922	2.031	22.32	117.3	-	-	-	-	-	-

Intel Core i5. We included the time taken to compute the persistence diagrams in the running times for our algorithm.

We also use synthetic data to empirically compare the running time of our algorithm to other dataset clustering algorithms available. Computing the Wasserstein distance has super-cubic time complexity Ling & Okada (2007), so is a significant bottleneck both for our algorithm and comparable Wasserstein barycentre clustering algorithms Benamou et al. (2015); Cuturi & Doucet (2014); Li & Wang (2008); Ye & Li (2014); Ye et al. (2017). Persistence diagrams generally reduce both the dimensionality and number of points in a dataset,⁵ so we in turn reduce the computational bottleneck. To demonstrate this, we evaluated the average time per iteration of our persistence diagram clustering algorithm, as well as the average iteration time for comparable Wasserstein barycentre clustering algorithms. We included the time taken to compute the persistence diagrams from the datasets when timing our clustering algorithm. We give the results in Table 3, leaving an entry blank where it became unpractical to run a test (e.g. it takes too long to return a solution and the algorithm becomes unresponsive). We show at least an order of magnitude improvement in performance over comparable Wasserstein barycentre clustering algorithms.

C.2 LATTICE STRUCTURES

The results obtained are in Tables 5-8. The fuzzy values for FPDCluster are given as floats, although in each case they converged to an absolute cluster. The Wasserstein barycentre clustering algorithms each have discrete labels. The correct labellings are for 1-3 and 4-6 to be clustered together in each case. We clustered the 2-PH diagrams. We denote a label as having been assigned by 1, or not assigned by 0. We ran each algorithm for five iterations. We obtained our datasets as cif files, converted them to xyz files, and then to csv files, producing a list of the coordinates of each atom in \mathbb{R}^3 . We create three copies of each structure. For rotation, we rotate two of them by 180° around different axes. For reflection, we reflect two of them in different axes. For translation, we translate them up or down by the length of the unit-cell. We use our own python implementation of FPDCluster, available in the supplementary materials. For each of the other algorithms, we use the implementation provided at https://github.com/bobje/WBC_Matlab, a copy of which is in the supplementary materials. We do not limit the number of points in the diagram when clustering.

C.3 DECISION BOUNDARIES

Why hard clustering does not work. In order to assign each task to the top-ranked models, we need to have a path from a task to the nearest cluster centre, then from that cluster centre to the k -nearest models (note that when we refer to models/tasks, we're implicitly referring to the persistence diagram of their decision boundary). We can always find that route when fuzzy clustering, as the fractional membership values mean that we have information about the proximity of every model/task with every cluster centre. However, with hard clustering we cannot always find that route. Firstly, the hard labelling means that you lose a lot of information about the proximity of models/tasks to cluster centres. Therefore, in order to find a route, we need a every task to be assigned to a cluster centre

⁵Persistence diagrams are always planar, so if the data is in \mathbb{R}^d , $d > 2$, then there is a dimensionality reduction. For $p > 0$, the persistence diagram of p -PH always has less points than the dataset when computed with the Vietoris-Rips complex.

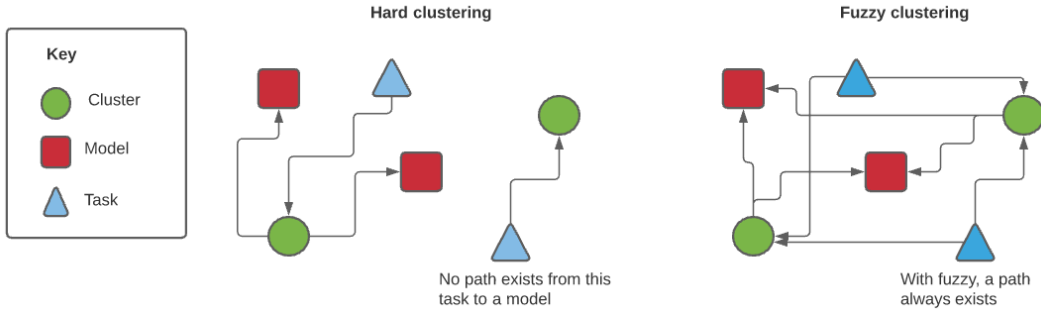


Figure 5: With hard clustering, we cannot always find a path from a task to a model.

that also has a model assigned to it. However, there are no guarantees that will happen. We show an example where no path exists in Figure 5.

Experimental details. All code used for computation is available in the supplementary materials. For models, we trained the standard Pytorch CNN available at <https://github.com/pytorch/examples/blob/master/mnist/main.py>. We trained them on MNIST, FashionMNIST, and KMNIST, each obtained using the Torchvision.datasets package. We split the data into 9 binary datasets for classification, class 0 vs each of the remaining classes. We trained three of each model, seeded with 0, 1, and 2 respectively. MNIST and KMNIST were each trained for five epochs, FashionMNIST was trained for 14 epochs. We used Ripser to compute the 1-persistence diagrams using default settings. We limited the number of points in the diagram to the 25 most persistent when clustering. Our percentage improvement values use the membership values after 16 iterations. We compute the standard error bounds when calculating the percentage improvement.

Table 4: Clustering results after transformation

	Cubic Structures				Carbon Allotropes			
	None	Rotate	Reflect	Translate	None	Rotate	Reflect	Translate
FPDCluster	✓	✓	✓	✓	✓	✓	✓	✓
ADMM	✓	✗	✓	✗	✓	✗	✗	✗
BADMM	✓	✗	✓	✗	✓	✗	✗	✗
SubGD	✓	✗	✓	✗	✓	✗	✗	✗
IterBP	✓	✗	✓	✗	✓	✗	✗	✗
LP	✓	✗	✓	✗	✓	✗	✗	✗

Table 5: Membership values for non-transformed datasets

		Cubic Structure Datasets						Carbon Allotrope Datasets					
		1	2	3	4	5	6	1	2	3	4	5	6
FPDCluster	Cluster 1	1.000	1.000	1.000	0.000	0.000	0.000	1.000	1.000	1.000	0.000	0.000	0.000
	Cluster 2	0.000	0.000	0.000	1.000	1.000	1.000	0.000	0.000	0.000	1.000	1.000	1.000
ADMM	Cluster 1	1	1	1	0	0	0	1	1	1	0	0	0
	Cluster 2	0	0	0	1	1	1	0	0	0	1	1	1
BADMM	Cluster 1	1	1	1	0	0	0	1	1	1	0	0	0
	Cluster 2	0	0	0	1	1	1	0	0	0	1	1	1
SubGD	Cluster 1	1	1	1	0	0	0	1	1	1	0	0	0
	Cluster 2	0	0	0	1	1	1	0	0	0	1	1	1
IterBP	Cluster 1	1	1	1	0	0	0	1	1	1	0	0	0
	Cluster 2	0	0	0	1	1	1	0	0	0	1	1	1
LP	Cluster 1	1	1	1	0	0	0	1	1	1	0	0	0
	Cluster 2	0	0	0	1	1	1	0	0	0	1	1	1

Table 6: Membership values for rotated datasets

		Cubic Structure Datasets						Carbon Allotrope Datasets					
		1	2	3	4	5	6	1	2	3	4	5	6
FPDCluster	Cluster 1	1.000	1.000	1.000	0.000	0.000	0.000	1.000	1.000	1.000	0.000	0.000	0.000
	Cluster 2	0.000	0.000	0.000	1.000	1.000	1.000	0.000	0.000	0.000	1.000	1.000	1.000
ADMM	Cluster 1	0	0	1	0	0	1	1	0	1	1	0	1
	Cluster 2	1	1	0	1	1	0	0	1	0	0	1	0
BADMM	Cluster 1	0	1	1	0	1	1	1	1	0	1	1	0
	Cluster 2	1	0	0	1	0	0	0	0	1	0	0	1
SubGD	Cluster 1	0	1	1	0	1	1	1	0	0	1	0	0
	Cluster 2	1	0	0	1	0	0	0	1	1	0	1	1
IterBP	Cluster 1	0	1	0	0	1	0	0	1	1	0	1	1
	Cluster 2	1	0	1	1	0	1	1	0	0	1	0	0
LP	Cluster 1	1	0	1	1	0	1	0	1	0	0	1	0
	Cluster 2	0	1	0	0	1	0	1	0	1	1	0	1

Table 7: Membership values for reflected datasets

		Cubic Structure Datasets						Carbon Allotrope Datasets					
		1	2	3	4	5	6	1	2	3	4	5	6
FPDCluster	Cluster 1	1.000	1.000	1.000	0.000	0.000	0.000	1.000	1.000	1.000	0.000	0.000	0.000
	Cluster 2	0.000	0.000	0.000	1.000	1.000	1.000	0.000	0.000	0.000	1.000	1.000	1.000
ADMM	Cluster 1	1	1	1	0	0	0	0	0	0	1	1	0
	Cluster 2	0	0	0	1	1	1	1	1	1	0	0	1
BADMM	Cluster 1	1	1	1	0	0	0	0	0	0	1	1	0
	Cluster 2	0	0	0	1	1	1	1	1	1	0	0	1
SubGD	Cluster 1	1	1	1	0	0	0	1	1	1	1	1	0
	Cluster 2	0	0	0	1	1	1	0	0	0	0	0	1
IterBP	Cluster 1	1	1	1	0	0	0	0	0	0	0	0	1
	Cluster 2	0	0	0	1	1	1	1	1	1	1	1	0
LP	Cluster 1	1	1	1	0	0	0	0	0	0	0	1	1
	Cluster 2	0	0	0	1	1	1	1	1	1	1	0	0

Table 8: Membership values for translated datasets

		Cubic Structure Datasets						Carbon Allotrope Datasets					
		1	2	3	4	5	6	1	2	3	4	5	6
FPDCluster	Cluster 1	1.000	1.000	1.000	0.000	0.000	0.000	1.000	1.000	1.000	0.000	0.000	0.000
	Cluster 2	0.000	0.000	0.000	1.000	1.000	1.000	0.000	0.000	0.000	1.000	1.000	1.000
ADMM	Cluster 1	0	0	1	0	0	1	0	0	1	0	0	1
	Cluster 2	1	1	0	1	1	0	1	1	0	1	1	0
BADMM	Cluster 1	0	1	0	1	1	0	1	1	0	1	1	0
	Cluster 2	1	0	1	0	0	1	0	0	1	0	0	1
SubGD	Cluster 1	0	0	1	0	0	1	0	1	0	0	1	0
	Cluster 2	1	1	0	1	1	0	1	0	1	1	0	1
IterBP	Cluster 1	0	1	0	0	1	0	0	0	1	0	0	1
	Cluster 2	1	0	1	1	0	1	1	1	0	1	1	0
LP	Cluster 1	0	0	1	0	0	1	1	0	1	1	0	1
	Cluster 2	1	1	0	1	1	0	0	1	0	0	1	0